Constraints Imposed by a High Magnetic Field on Models for the EUV Emission in the Coma Cluster

Ming Yann Tsay and Chorng-Yuan Hwang

Graduate Institute of Astronomy, National Central University, Taiwan

hwangcy@astro.ncu.edu.tw

and

Stuart Bowyer

Space Sciences Laboratory, University of California, Berkeley, CA 94720-7450

ABSTRACT

A variety of models have been explored in regard to the origin of the excess extreme ultraviolet ($\sim 0.1~\rm keV$) emission in the Coma cluster. It is now established that the flux is non-thermal and the only non-thermal source mechanism that appears viable is inverse Compton emission produced by $\sim 100~\rm MeV$ electrons interacting with the cosmic microwave background photons. All but one of the models that have been proposed require a cluster magnetic field $< 1\mu\rm G$. However, recent observations strongly suggest the magnetic field in the Coma cluster is $\sim 5\mu\rm G$. We investigate the constraints on models imposed by a $5\mu\rm G$ cluster field and find a limited class of models that are compatible with this constraint. We also investigate the possibility that the excess hard (40-60 keV) X-ray emission in the cluster is produced by inverse Compton emission with the same electron population that produces the EUV excess. We find no scenarios that are compatible with a large cluster magnetic field, and consequently in this case these two components must be unrelated.

Subject headings: galaxies: clusters: individual(Coma)—magnetic fields—radiation mechanisms: non-thermal

1. INTRODUCTION

EUV emission in the Coma cluster in excess of that produced by the thermal X-ray gas was first reported by Lieu et al. (1996). Further analysis of data on this cluster was

carried out by Bowyer and Berghöfer (1998) and Bowyer et al. (1999). Initially, this flux was attributed to thermal emission from "warm" gas at 10⁶ K. Maintenance of a warm intracluster gas is extraordinarily difficult, and on these grounds alone it was generally agreed that a thermal source was untenable. Observations relevant to this issue were obtained with the Hopkins Ultraviolet telescope (Dixon et al. 1996), and FUSE (Dixon et al. 2001a,b). No Far UV line emission from gas at 10⁶ K was detected. More recently, observations of several clusters with XMM (Tamura et al. 2001; Kaastra et al. 2001; Peterson et al. 2001) have shown no evidence for a 10⁶ temperature gas. All additional clusters examined with XMM also show no evidence for a "warm" 10⁶ gas (S. Kahn, private communication). The sum of all these findings seems compelling: a thermal mechanism for the EUV excess can be ruled out. (However, for an alternate point of view see Mittaz et al. 1998; Lieu, Bonamente, & Mittaz 1999; Lieu et al. 1999; Lieu, Bonamente, & Mittaz 2001a,b.)

Since the source mechanism is not thermal, it must be the product of a non-thermal process. Inverse Compton scattering (ICS) of cosmic rays with the 2.7 K cosmic microwave background was suggested early-on as a possible source mechanism (Hwang 1997; $\text{En}\beta$ lin & Biermann 1998). This is the only non-thermal mechanism that has been suggested as a possibility for the source of this flux.

A number of researchers have explored models of ICS in an attempt to explain the EUV excess in the Coma cluster (Hwang 1997, Bowyer & Berghöfer 1998, En β lin & Biermann 1998, Sarazin 1999, Atoyan & Völk 2000, Brunetti et al. 2001). With one exception (Atoyan & Völk 2000), all of these models require a low ($< 1\mu$ G) field and typically these models require a very low magnetic field ($< 0.5\mu$ G) field.

A hard (25-80 keV) X-ray flux in excess of that produced by the 10⁸ K thermal X-ray gas has been detected with observations with BeppoSAX (Fusco-Femiano et al. 1999). Brunetti et al. (2001) have attempted to explain both the EUV and hard X-ray excesses in Coma by a single complex model. This model also employed a low magnetic field.

New studies of the magnetic field in clusters of galaxies strongly suggest that magnetic fields in clusters of galaxies are $\sim 5\mu G$. In this paper we investigate constraints imposed by a high magnetic field on models capable of producing the EUV excess in clusters of galaxies via the ICS process. We also briefly consider the effects of a high magnetic field on attempts to produce both the EUV and the hard X-ray emission by the ICS mechanism with the same population of cosmic ray electrons.

2. ASSUMPTIONS AND OVERALL APPROACH

We make the following assumptions.

- A.) The magnetic field is 5μ G. The magnetic field in the Coma cluster has been the subject of considerable study and observational results vary considerably. Estimates based in part on equipartition arguments typically result in low field estimates (Rephaeli 1988, Giovannini et al. 1993). However, recent observational results strongly indicate that cluster magnetic fields are quite large. Clarke et al. (2001) studied sixteen clusters; a substantial number of data points were obtained for each cluster. They found the cluster magnetic fields were all in the range $\sim 4-7\mu G$. These results seem compelling, but it could be argued that they are not applicable to the Coma cluster since that cluster was not included in their study. However, the Coma cluster field can be determined by a different procedure albeit for only one location in the cluster. Feretti et al. (1995) studied the rotation measure of the cluster-embedded head-tail radio source NGC 4869 (5C4.81). They found the number of magnetic field reversals through the cluster > 200 indicating B $> 4.9\mu$ G. This measurement is limited by the resolution of the VLA configuration employed and, in principle, is a lower limit for the number of magnetic field reversals through the cluster. It is possible that with even higher resolution the number of magnetic field reversals through the cluster could be larger, with a resulting increase in the estimate of B. However, this estimate is within the 4 to 7 μ G range found by Clarke et al. (2001) for all clusters in their sample. In view of these observations, we find the assumption of $5\mu G$ for the field in the Coma cluster to be quite reasonable.
- B.) A scattering process is operative in the cluster which will result in a sufficiently long path length for the electrons that the deposition of the energy of the electrons occurs within the cluster itself. We note there is overwhelming observational support for this assumption since if the cosmic rays did not deposit their energy within the cluster, they would escape the cluster and produce excess EUV emission over a region which is far larger than the cluster itself.
- C.) We assume the evolution of the electron population is given by the equation (Sarazin 1999):

$$\frac{\partial N(\gamma)}{\partial t} = \frac{\partial [b(\gamma)N(\gamma)]}{\partial \gamma} + Q(\gamma) \tag{1}$$

where $N(\gamma)d\gamma$ is the total number of electrons in the range γ to $\gamma + d\gamma$, $b(\gamma)$ is the energy loss rate of an electron with energy of γ , $Q(\gamma)d\gamma$ is the injection rate of electrons in the energy range γ to $\gamma + d\gamma$.

D.) We assume the injected cosmic-ray electrons follow a power law distribution.

E.) We assume the only energy loss mechanisms are inverse Compton emission, synchrotron radiation, Coulomb ionization and bremsstrahlung.

The energy loss rate for relativistic electrons interacting with the cosmic microwave background is given by Longair (1994):

$$b_{IC}(\gamma) = \frac{4}{3} \frac{\sigma_T}{m_e c} \gamma^2 U_{CMB} = 1.37 \times 10^{-20} \gamma^2 s^{-1}$$
 (2)

where σ_T is the Thomson cross section and U_{CMB} is the energy density of the cosmic microwave background. The loss rate by synchrotron emission is given by Longair (1994):

$$b_{syn}(\gamma) = \frac{4}{3} \frac{\sigma_T}{m_e c} \gamma^2 U_B = 1.30 \times 10^{-21} \gamma^2 (\frac{B}{1\mu G})^2 \text{s}^{-1}$$
 (3)

where B is the magnetic field and $U_B = B^2/8\pi$ is the energy density of the magnetic field. The loss rate for Coulomb ionization is given by Sarazin (1999):

$$b_{Coul}(\gamma) \sim 1.2 \times 10^{-12} n_e \left[1.0 + \frac{\ln(\gamma/n_e)}{75} \right] \text{s}^{-1}$$
 (4)

where n_e is the thermal electron density in the ICM of the Coma cluster. The loss rate for the Bremsstrahlung is approximately (Sarazin 1999):

$$b_{brem}(\gamma) \sim 1.51 \times 10^{-16} n_e \gamma [\ln(\gamma) + 0.36] \text{s}^{-1}$$
 (5)

A comparison of the energy loss rates for these four mechanisms is given in Fig.1. This shows that ICS is the dominant energy loss rate mechanism for relativistic electrons in a 0.2μ G cluster field while synchrotron radiation is the main energy loss rate process for relativistic electrons in 5μ G cluster field. A diagram of the energy loss rate timescale $\gamma/(b_{IC} + b_{syn} + b_{Coul} + b_{brem})$ versus electron energies is shown in Fig.2. Note that there is a decrease of 10% in the energy of the peak energy loss, and, more importantly, there is a decrease in the peak energy loss rate of $\sim 40\%$ for the case of a 5μ G field as compared to a 0.2μ G field.

The observed EUV ICS flux is given by Blumenthal & Gould (1970):

$$f_{IC}(\epsilon) = \frac{1}{4\pi D^2} \times \frac{r_o^2}{\hbar^3 c^2 \pi} \times K_e \times (kT)^{\frac{p+5}{2}} \times F(p) \times \epsilon^{-\frac{p+1}{2}},\tag{6}$$

where the symbols have their standard meaning. The energy of the photon observed, ϵ , has been obtained by folding the effective area of the EUVE Deep Survey Telescope (Sirk et al. 1997) with absorption of EUV emission by the Galactic interstellar medium in the direction

of Coma following the prescription of Bowyer et al. (1999). The peak of the resultant telescope effective area is at 80 Å.

The synchrotron radio flux is given by Blumenthal and Gould (1970):

$$f_{syn}(\nu) = \frac{1}{4\pi D^2} \times \frac{4\pi e^3}{m_e c^2} \times K_e \times B^{\frac{p+1}{2}} \times \left(\frac{3e}{4\pi m_e c}\right)^{\frac{p-1}{2}} \times a(p) \times \nu^{\frac{-p+1}{2}}.$$
 (7)

We have used an integrated diffuse flux density for Coma C of 640 mJy at 1.4 GHz (Deiss et al. 1997) in combination with a spectral index $\alpha = (p-1)/2 = 1.16$ (Bowyer & Berghöfer 1998) as our observational base.

We investigate three scenarios. In the first, we consider a large injection event occurring over a relatively short time which produces the cosmic-ray electron population. In the second scenario, we assume a continuous sequence of small injection events. Finally, we consider a combination of these two: a large injection event followed by continuous smaller events. In Table 1 we show the input parameters for these three models.

In this Table, N_o is the normalization factor and p is the spectral index of the initial injected rate. Q_o refers to the normalization factor and p' is the spectral index of the continuous injection rate. Q_o is related to the injected electron number Q by the relation $Q = Q_o \times \gamma^{-p'}$. n_e is the thermal electron density in the ICM. EI denotes the energy input.

3. RESULTS

We first consider the case of a single primary injection event. The results with input parameters from Model 1 are shown in Fig.3. This population will produce the EUV emission as reported by Bowyer et al. (1999) shown as a cross. This population greatly overproduces the observed synchrotron radio emission which is shown as a heavy solid line in the figure. With the passage of time, synchrotron losses degrade the higher energy electrons, and the resultant population after 1.4×10^8 yr and after 2.5×10^8 yr is shown by line A and by line B respectively. The results shown in this figure demonstrate why it is not possible to produce both the EUV and the radio emission by a population of electrons produced in a single initial event.

We next consider the case of a continuous distribution of smaller events. The results with the input parameters from Model 2 are shown in Fig.4. The dashed line shows the total injected electrons. The thin solid line shows the electron population after 2×10^9 yr. The heavy solid line shows the distribution of the electrons that are required to produce the observed synchrotron radio emission and the cross shows the distribution of the electrons

producing the observed EUV emission. The results shown in this figure show why no uniform continuous distribution of injection events can reproduce the observational data.

We have independently derived a variety of electron populations using a cluster field of 0.2μ G; these are all capable of reproducing the EUV and radio observations. This is consistent with results found by a number of previous studies that demonstrated that a continuous distribution of injection events can produce populations that will replicate both the EUV and the radio data in the case of low cluster fields.

We next consider a primary event followed by continuous injections. We use input parameters listed in Models 3 through 11. The population obtained using the parameters in Model 3 after an evolution time of 1 Gyr are shown as a dashed line in Fig.5. We also show the effect of changes in the size of the initial event. These results are shown as line A and employ inputs from Model 4. Finally, we show the effect of changes in p. Using inputs taken from Model 5, we obtain the population shown as line B.

In Fig.6 we show the effect of changes in Q_o and in the spectral index of the electrons in the input events, p', on the overall electron population. The inputs for the dashed line are from Model 3. Line A shows the results of decreasing the spectral index using inputs from Model 6. Line B shows the results of decreasing Q_o using inputs of Model 7. The results in this figure show that allowed variations in Q_o and p' are quite small since even modest changes in one of these parameters alone will result in an electron population that cannot produce the radio data.

We have investigated the extent to which we can mimic the best fit electron population shown in Model 3 by models which change p' and Q_o (the continuous injections). Inputs are shown in Model 8 and 9. The resultant electron distributions are shown in Fig.7. As can be seen there is only a limited amount of freedom in constructing this type of model since large changes in these offsetting parameters which can be used to fit the EUV data will quickly destroy the fit to the radio data. Good fits will be obtained if p' is ~ 2.32 .

In Fig.8 we show the effect of different thermal electron densities on the cosmic ray electron population. The dashed line is the product of the inputs in Model 3; the solid line is the result using the inputs in Model 10. The electron densities in this model are an order of magnitude smaller than those in Model 3. As can be seen, the cosmic ray electron population is not greatly sensitive to changes in the thermal electron density in the higher energy range.

In Fig.9 we show the constraints imposed on the time of the initial event in our composite model. The input parameters are from Model 3. The dashed line corresponds to an evolutionary time of 1 Gyr, and the solid line is the electron population after 1.4 Gyr.

We also investigated the effect of a 5 μ G field with regards to the hypothesis that both the EUV excess and the high energy X-ray flux are produced by the ICS mechanism with the same population of electrons. In this work we used Models 3, 8, 9, 10, and 11 which are capable of reproducing both the EUV and synchrotron radio flux. We investigated whether any of these models were also capable of producing the high energy X-ray flux by the ICS mechanism. The results are shown in Fig.10. In this figure, the top line is the observed excess hard energy flux (Rephaeli et al. 1999). The lower lines are the fluxes produced by the ICS mechanism in all five models. The flux produced by the ICS mechanism in all of these models is more than two orders of magnitude below the observed flux. Changes in the input characteristics of the injection events in these different models do not affect the predicted flux significantly.

4. DISCUSSION AND CONCLUSIONS

Atoyan & Völk (2000) are the only authors who have explored the production of an EUV excess in a high ($\geq 1\mu G$) intracluster field. They explored a model which is different in formal concept from those considered here, but is similar in form to our model with a large primary event followed by smaller injections. In specific, they considered two populations of cosmic rays. One is an old, highly evolved population which has undergone re-acceleration and compression; this population produces the EUV emission. A second higher energy population of cosmic rays which has been produced more recently by secondary origin is invoked to produce the radio emission. While this model may be appropriate, we note that models invoking secondary electrons for the radio emission have not been successful in producing the pronounced steeping of the spectral index of the radio emission with increasing distance from the cluster center that has been observed in well-studied radio halos such as Coma and Perseus. It has not been demonstrated that the Atoyan & Völk model can surmount this obstacle.

In this work we have studied general classes of models to establish which of these are capable of producing both the EUV and the synchrotron radio emission in a 5μ G cluster field. We studied models with a single initial event, models with continuous injection events, and combinations of these two. We find that in all models with just a single initial event, either the EUV emission will be underproduced or the synchrotron radio emission will be overproduced depending on the size of the event. With the passage of time, synchrotron losses (which are dominant in the high field case) will remove the higher energy components of the initial electron population, but the distribution required to produce the synchrotron radio emission is not produced. This problem is basic to all models with a single electron

injection event. Continuous models encounter a different problem. An electron spectrum can be constructed which will produce the synchrotron radio emission. However, this population is not capable of producing the EUV flux.

The combination of a primary event followed by smaller continuous events can produce the required electron distribution. However, the initial event must have occurred at a time no earlier than 1.4 Gyr in the past or the higher energy electrons will have been lost and insufficient EUV flux will be produced. The electron energy loss rate is sufficiently steep that even substantially increasing the number of electrons in the initial event will not substantially change this time constraint. On the other hand, the time of the initial event must be no more recent than 1 Gyr ago or the synchrotron radio emission will be overproduced. This requires that the injection event must have occurred in the time span 1.4 Gyr < injection < 1 Gyr.

Finally, we investigated the effects of a $5\mu G$ field if both the EUV excess and the high energy X-ray flux are produced by ICS mechanism with the same population of electrons. The results shown in Figure 10 show that the high energy X-ray emission produced via the ICS process falls far short of the observed flux for all of these models. We conclude it is impossible to produce both the EUV flux and the hard X-ray emission by ICS from the same population of electrons with reasonable electron injection scenarios. We note that Atoyan & Völk (2000) have reached similar conclusions.

The project is supported by the National Science Council of Taiwan (grant number NSC 90-2112-M-008-040) and the Graduate Institute of Astronomy, NCU. S.B. thanks the faculty and staff of the Graduate Institute of Astronomy, NCU, and the National Center for Theoretical Science of Taiwan for their support and warm hospitality during an extended stay.

REFERENCES

Atoyan, A., & Völk, H. 2000, ApJ, 535, 45

Blumenthal, G. R., & Gould, R. J. 1970, Rev. Mod. Phys., 42, 237

Bonamente, M., Lieu, R., & Mittaz, J. 2001a, ApJ, 546, 805

Bonamente, M., Lieu, R., & Mittaz, J. 2001b, ApJ, 547, 7

Bowyer, S., & Berghöfer, T. 1998, ApJ, 506, 502

Bowyer, S., Berghöfer, T. W., & Korpela, E. J. 1999, ApJ, 526, 592

Brunetti, G., Setti, G., Feretti, L., & Giovannini, G. 2001, New Astronomy, 6, 1

Clarke, T., Kronberg, P., & Böhringer, H. 2001, ApJ, 547, L111

Deiss, B.M., Reich, W., Lesch, H., & Wielebinski, R. 1997, A&A, 321, 55

Dixon, W. V. D., Hurwitz, M., & Ferguson, H. 1996, ApJ, 469, L77

Dixon, W. V. D., Sallmen, S., Hurwitz, M., & Lieu, R. 2001a, ApJ, 550, L25

Dixon, W., Sallmen, S., Hurwitz, M., & Lieu, R. 2001b, ApJ, 552, L69

 $\text{En}\beta \text{lin}, \text{ T. A.}, \& \text{ Biermann}, \text{ P. L. 1998}, \text{ A&A}, 330, 90$

Feretti, L., Dallacasa, D., Giovannini, G., & Tagliani, A. 1995, A&A, 302, 680

Fusco-Femiano, R., Dal Fiume, D., Feretti, L., Giovannini, G., Grandi, P., Matt, G., Molendi, S., & Santangelo, A. 1999, ApJ, 512, L21

Giovannini, G., Feretti, L., Venturi, T., Kim, K.-T., & Kronberg, P. P. 1993, ApJ, 406, 399

Hwang, C.-Y. 1997, Science, 278, 1917

Kaastra, J. S., Ferrigno, C., Tamura, T., Paerels, F. B. S., Peterson, J. R., & Mittaz, J. P. P. 2001, A&A, 365, L99

Lieu, R., Mittaz, J., Bowyer, S., Breen, J., Lockman, F., Murphy, E., & Hwang, C.-Y. 1996, Science, 274, 1335

Lieu, R., Bonamente, M., & Mittaz, J. 1999, ApJ, 517, 91

Lieu, R., Bonamente, M., Mittaz, J., Durrett, F., Dos Santos, S., & Kaastra, J. 1999, ApJ, 527, 77

Lieu, R., Bonamente, M., & Mittaz, J. 2000, A&A, 364, 497

Longair, M. S. 1994, High Energy Astrophysics, Vol. 2, Cambridge University Press

Mittaz, J., Lieu, R., & Lockman, F. 1998, ApJ, 498, 17

Peterson, J. R., Paerels, F. B. S., Kaastra, J. S., Arnaud, M., Reiprich, T. H., Fabian, A. C., Mushotzky, R. F., Jernigan, J. G., & Sakelliou, I. 2001, A&A, 365, L104

Rephaeli, Y. 1988, Comments on Modern Physics, Part C, 12, 265

Rephaeli, Y., Gruber, D., & Blanco, P. 1999, ApJ, 511, L21

Sarazin, C. L. 1999, ApJ, 520, 529

Sirk, M., Vallerga, J., Finley, D., Jalensky, P., & Malina, R. 1997, ApJ, 110, 347

Tamura, T., Kaastra, J. S., Peterson, J. R., Paerels, F. B. S., Mittaz, J. P. D., Trudolyubov, S. P., Stewart, G., Fabian, A. C., Mushotzky, R. F., Lumb, D. H., & Ikebe, Y. 2001, A&A, 365, L87

This preprint was prepared with the AAS $\mbox{\sc LAT}_{\mbox{\sc E}}\mbox{\sc X}$ macros v5.0.

Table 1.

Model	N_o	p	EI(erg)	$Q_o\left(\mathbf{s}^{-1}\right)$	p'	$EI(erg yr^{-1})$	$n_e(\mathrm{cm}^{-3})$
Single Primary Event							
No.1	5.5×10^{67}	2.32	1.64×10^{61}				3×10^{-3}
Continuous Injection							
No.2	2×10^{49}	2.32	5.96×10^{42}	2×10^{49}	2.32	1.88×10^{50}	3×10^{-3}
Primary Event Followed by Continuous Injection							
No.3	9×10^{67}	2.32	2.68×10^{61}	2×10^{49}	2.32	1.88×10^{50}	3×10^{-3}
No.4	9×10^{68}	2.32	2.68×10^{62}	2×10^{49}	2.32	1.88×10^{50}	3×10^{-3}
No.5	9×10^{67}	2.5	6.87×10^{60}	2×10^{49}	2.32	1.88×10^{50}	3×10^{-3}
No.6	9×10^{67}	2.32	2.68×10^{61}	2×10^{49}	2.2	4.80×10^{50}	3×10^{-3}
No.7	9×10^{67}	2.32	2.68×10^{61}	2×10^{48}	2.32	1.88×10^{49}	3×10^{-3}
No.8	9×10^{67}	2.32	2.68×10^{61}	8×10^{48}	2.2	1.92×10^{50}	3×10^{-3}
No.9	9×10^{67}	2.32	2.68×10^{61}	9×10^{49}	2.5	2.17×10^{50}	3×10^{-3}
No.10	9×10^{67}	2.32	2.68×10^{61}	2×10^{49}	2.32	1.88×10^{50}	3×10^{-4}
No.11	3.5×10^{68}	2.5	2.67×10^{61}	2×10^{49}	2.32	1.88×10^{50}	3×10^{-3}

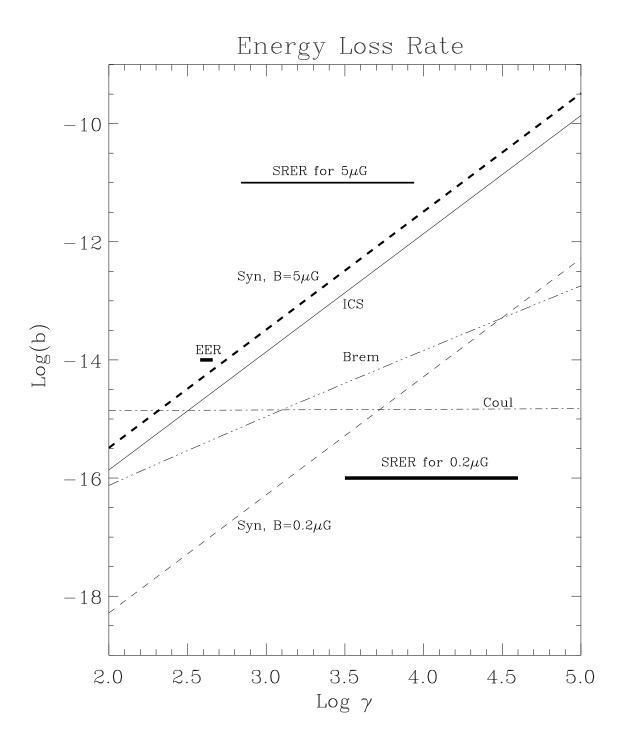


Fig. 1.— Energy loss rates for individual mechanisms including inverse Compton scattering (ICS), synchrotron radiation (Syn) in two magnetic fields, Coulomb ionization (Coul), and bremsstrahlung radiation (Brem). EER is the "EUV-emitting electron range" and SRER is the "synchrotron-radio-emitting electron range".

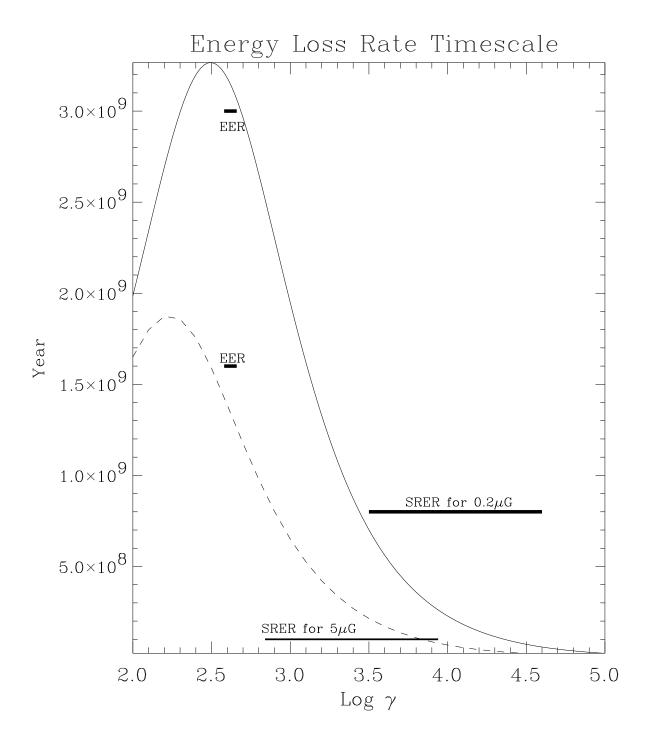


Fig. 2.— The energy loss rate timescale for the electrons in a 5μ G and 0.2μ G field. The dashed line is the timescale for 5μ G case and the solid line is for 0.2μ G. The thick horizontal lines mark the EUV-emitting electron range and the synchrotron-radio-emitting electron range.

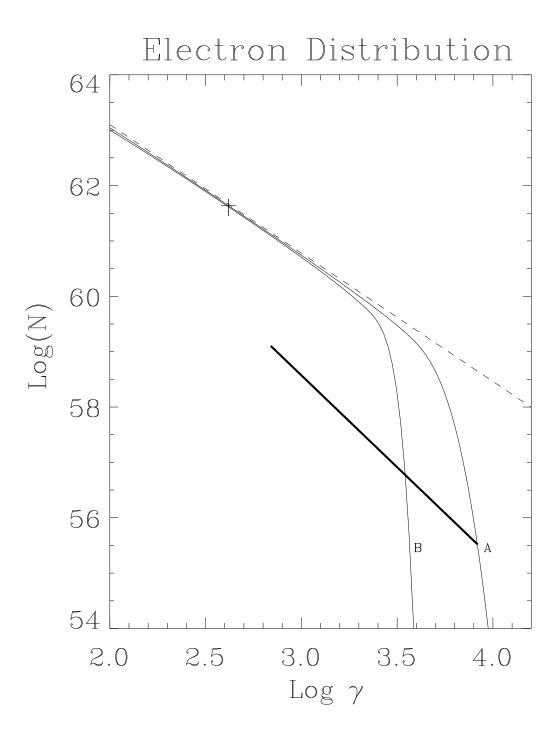


Fig. 3.— The electron spectrum using the inputs in Model 1. The dashed line shows the distribution of the initial injected electrons. Line A shows the distribution of the electrons after 1.4×10^8 yr while line B shows the distribution after 2.5×10^8 yr. The cross is the distribution of the electrons producing the observed EUV flux and the heavy solid line is the distribution of the electrons producing the synchrotron radio emission.

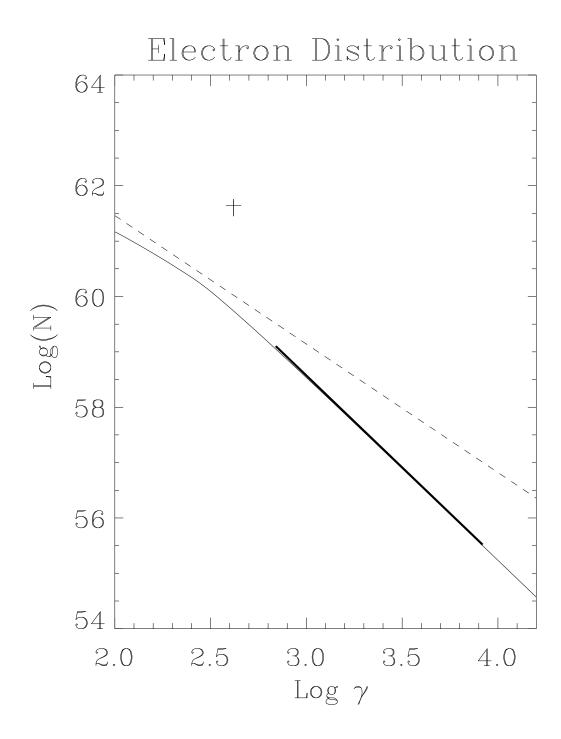


Fig. 4.— The electron spectrum using the inputs in Model 2 with an evolution time of 2×10^9 yr. The dashed line shows the total injected electrons.

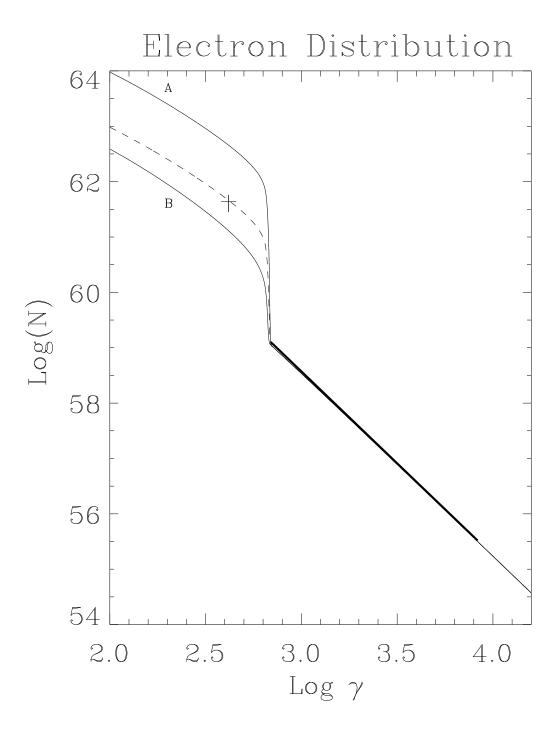


Fig. 5.— The dashed line shows the electron distribution using inputs from Model 3 with an evolution time of 1 Gyr. Line A with input parameters from Model 4 shows the distribution of electrons with N_o increased, and line B with input parameters from Model 5 shows the distribution of the electrons with p increased.

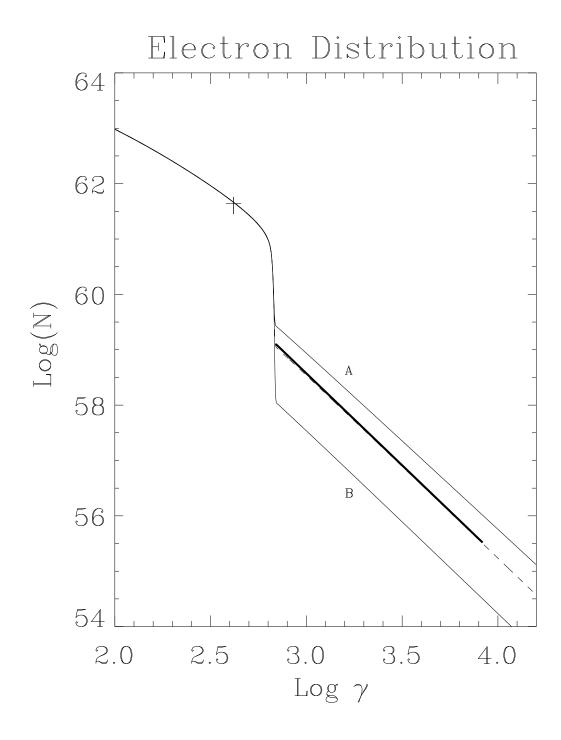


Fig. 6.— The effects of changes in Q_o and p' on the electron spectrum. The dashed line is Model 3. Line A shows the results of decreasing p' using the input parameters of Model 6. Line B shows the results of decreasing Q_o using the inputs in Model 7. The evolution time is 1 Gyr.

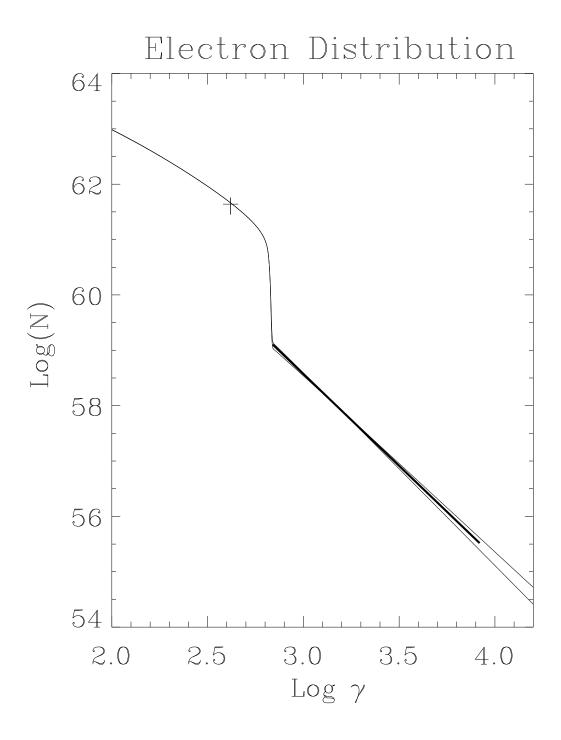


Fig. 7.— Models mimic the best fit electron distribution (Model 3). 2.2 and 2.5 are chosen for p' and the resultant electron distributions are shown as the solid lines. The evolution time is 1 Gyr.

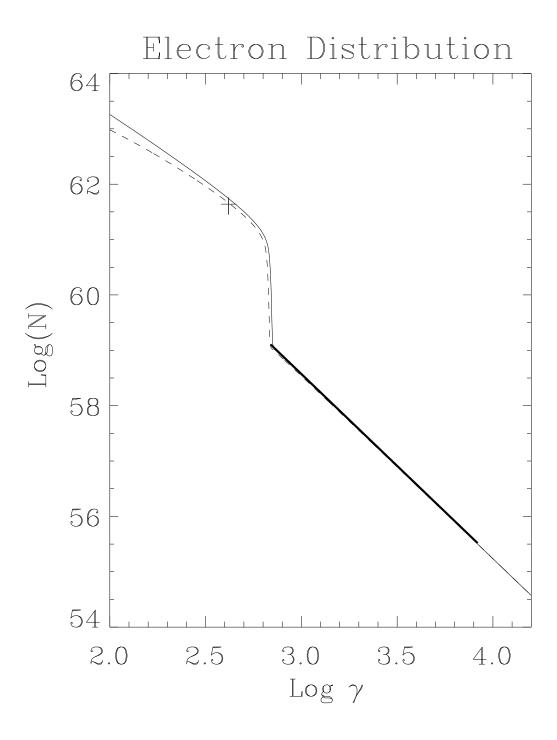


Fig. 8.— The effect of differing thermal electron densities, n_e . The dashed line is the product of the inputs in Model 3; the solid line is the result using the inputs from Model 8 with n_e smaller by a factor of 10. The evolution time is 1 Gyr.

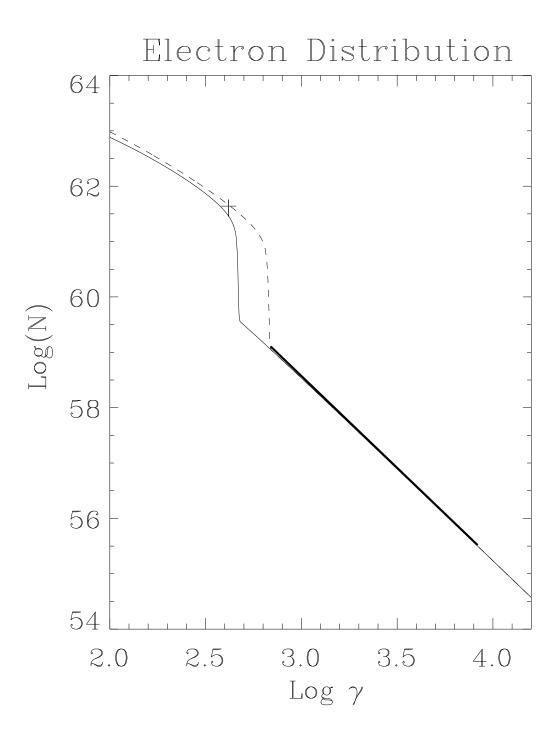


Fig. 9.— The effect of different evolution times. The input parameters are from Model 3. The dashed line is the distribution after 1 Gyr and the solid line is the distribution after 1.4 Gyr.

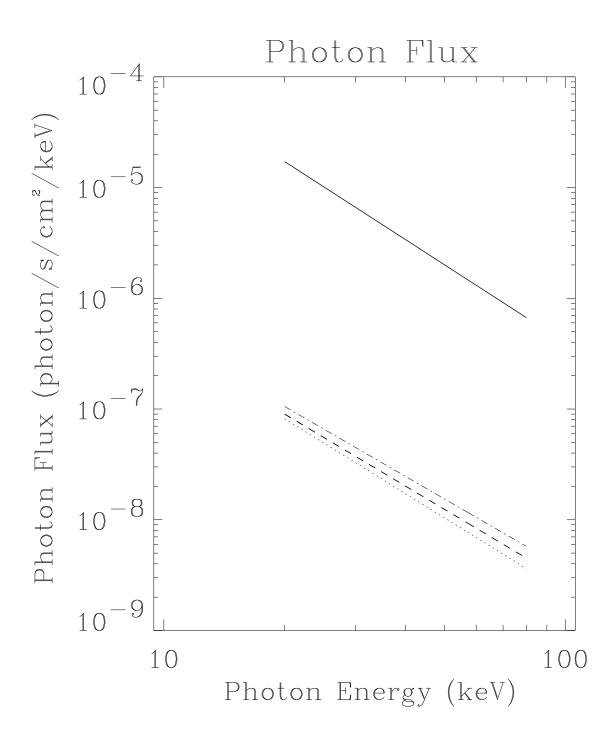


Fig. 10.— A comparison of the observed hard X-ray flux and the ICS results of the models. The solid line shows the excess high energy X-ray flux. The dashed line shows the flux produced by the ICS mechanisms using inputs from Model 3, 10, and 11. The emission predicted by these three models is virtually the same. The dash-dot line shows the emission predicted by Model 8, and the dotted line shows the emission predicted by Model 9.